Modal symmetries at the nanoscale: a route towards a complete vectorial near-field mapping

Boris le Feber,[1] Nir Rotenberg,[1] Dries van Oosten,[2] and L. Kuipers[1,*]

[1] *Center for Nanophotonics, FOM Institute AMOLF, Science Park 104, 1098 XG Amsterdam, The Netherlands*
[2] *Debye Institute for Nanomaterials Science, Utrecht University, P.O. Box 80000, 3508 TA Utrecht, The Netherlands*
[*] *Corresponding author: kuipers@amolf.nl*

Compiled April 28, 2014

We use symmetry considerations to understand and unravel near-field measurements, ultimately showing that we can spatially map three distinct fields using only two detectors. As an example, we create two-dimensional field maps of the out-of-plane magnetic field and two in-plane fields for a silicon ridge waveguide. Furthermore, we are able to identify and remove polarization mixing of less than 1/30 of our experimental signals. Since symmetries are prevalent in nanophotonic structures and their near fields, our method can impact many future near-field measurements.

OCIS codes: 180.4243, 350.4238, 230.7370.

Most structures, be they naturally occurring crystals or artificial nanophotonic objects, posses some degree of symmetry. In fact, we often rely on these symmetries, to predict the flow of light about these structures. For example, structural symmetries are essential to the elegance of Mie scattering theory [1], or to the existence of photonic bandgaps [2]. Surprisingly, with few notable exceptions [3–5], the prevalent symmetries of nanophotonic structures have not been exploited in the analysis of near-field optical measurements.

Due to the tight confinement of light in nanophotonic structures, in the vicinity of these structures typically all six components of the optical near field - the three electric and the three magnetic - are nonzero. However, polarization-resolved near-field scanning optical microscopy (NSOM), be it in collection [6–8] or scattering [9–12] mode, allows for the simultaneous detection of only two orthogonally polarized channels. As we have recently shown, with those two channels it is possible to measure four field components [13]. Although in this case only two electromagnetic (EM) fields are missing, the separation of the signals into maps of the individual EM components is far from trivial. In fact, to date such a separation has not been demonstrated.

As is often the case, the underlying symmetry of photonic structures constrains their near fields, and can therefore help unravel near-field measurements. For example, on planes of symmetry, such as the center of a waveguide or nanoantenna, certain near-field components are identically zero. For the nanoantenna, a careful measurement of two nonzero field components was sufficient to create full EM field maps on the symmetry plane [3]. Likewise, measuring along the center of a ridge waveguide allowed for direct observations of the out-of-plane magnetic field using a split ring aperture probe (SRP) [4]. These examples, however, are limited to a single plane, whereas the constraints imposed by symmetry apply over all space.

In this Letter we demonstrate how knowledge of the symmetry of the structure and its associated fields can be used to unravel aperture NSOM measurements and create comprehensive two-dimensional near-field maps. We begin by showing how, for a benchmark photonic structure such as a ridge waveguide, we can use symmetry considerations to identify and correct for polarization mixing as small as 1/30 of our signals. Furthermore, we show that when we use a SRP to measure on this structure, we can unravel our measurements and create two-dimensional maps of three signals while using only two detectors.

To test our new methodology we measure on a benchmark photonic structure. Specifically, we use a 20 nm high, 2 μm wide ridge waveguide, that is mirror symmetric about the yz-plane (Fig. 1a). Using a commercial full wave solver (COMSOL), we find that at a free space wavelength of 1550 nm this structure supports a single TE mode ($n_{\text{eff}} = 1.65$). In Fig. 1b we show a snapshot in time of the calculated electric and magnetic components of the fields associated with the TE mode. We choose the point in time where E_x is completely real. At this instant all components are either completely real or completely imaginary. Around the center of the waveguide, E_x, H_y and H_z have an even symmetry, whereas E_y, H_x and E_z have an odd symmetry [14]. Noteworthily, the field profiles of both the even E_x and H_y and the odd E_y and H_x are very similar. The similarity between the in-plane electric and magnetic fields is further underlined by the observation that the ratio of the amplitude of E_x to E_y is close to the ratio of H_y to H_x.

These near fields can be converted to far-field radiation with a near-field probe that is in close proximity of the sample. We ensure x- and y- oriented electric near fields radiate to electric far-fields polarized along x and y (Fig 1a) [4], resulting in the signals L_x and L_y, respectively. However, the conventional aperture probe (AP) converts not only the in-plane electric, but also the in-plane magnetic near fields to far-field radiation [13]. In fact, radiation from H_y (H_x) has its electric field along

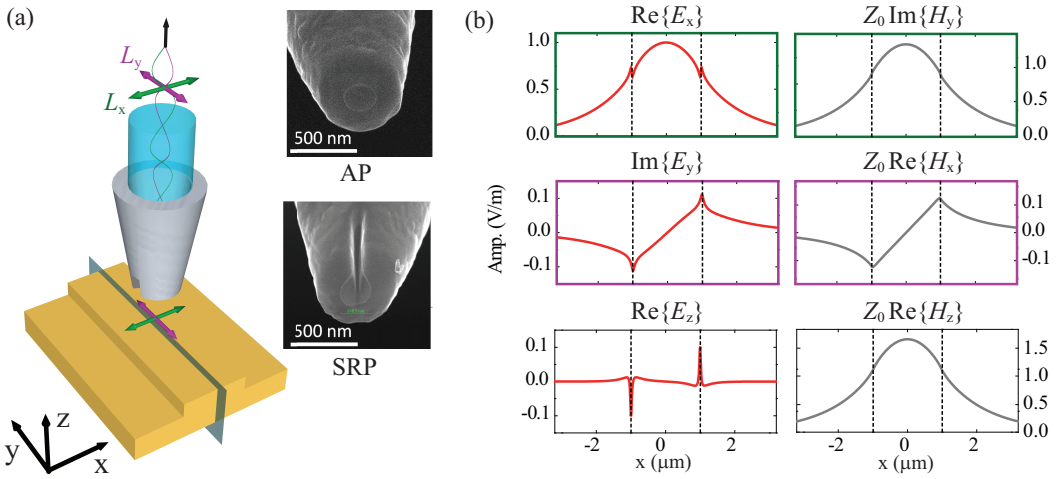

Fig. 1. (Color online) (a) A sketch of the sample and the tip of the SRP used in this work. The fiber forms the core of the tip. The green and purple arrows near the sample indicate electric fields along x and y. The probe converts these fields to radiation polarized along x and y, indicated by the top purple and green arrows. The polarization resolved detection of this radiation results in the signals L_x and L_y. The semi-transparent plane denotes the mirror symmetry of the waveguide (yz-plane). The inset shows scanning electron microscope images of the AP and the SRP. (b) Calculated field profiles 20 nm above the structure. To indicate to which detection channel the far-field radiation from these fields contributes, the borders of the plot windows are color coded to match the colors of field orientations shown in (a). The magnetic fields are multiplied by the free space impedance Z_0 and the amplitude of all fields is normalized to the maximum of E_x. The dashed black lines indicate the edges of the ridge.

x (y) and hence will be detected on the same detector as E_x (E_y). An additional component can be detected by using a SRP (inset of Fig. 1a). This probe converts not only the four in-plane fields, but also the out-of-plane magnetic field (H_z) into radiation to the detectors [4].

Before turning to the SRP, we apply the field symmetry constraints to unravel the data collected with an AP (inset of Fig. 1a). An example of such a measurement is shown in Fig. 2, where in the top panels of part (a) and (b) we show the 2D maps corresponding to the real part of the complex signals L_x and L_y, respectively. For the situation depicted in this figure we can write:

$$L_x = \alpha_x E_x + \beta_x Z_0 H_y \approx \alpha'_x E_x, \tag{1a}$$

$$L_y = \alpha_y E_y + \beta_y Z_0 H_x \approx \alpha'_y E_y, \tag{1b}$$

where the complex parameters α and β quantify the sensitivity to experimental electric and magnetic fields. We multiply the magnetic fields by the free space impedance Z_0, because we detect the electric field associated with this magnetic field. Furthermore, both the amplitude and profile of the calculated E_x (E_y) and H_y (H_x) are very similar (Fig. 1) and their ratio is constant over all space to within experimental accuracy. That is, $Z_0 H_{y,x}/E_{x,y} \approx p$ (where p is complex) and in Eq. 1 we use $\alpha'_{x,y} = \alpha_{x,y} + p\beta_{x,y}$ to express the signals in terms of $E_{x,y}$ alone.

The fields maps shown in the top panels of Fig. 2a and b suggest that indeed a AP largely collects the signals predicted by Eq. 1. Not only does L_x appear to have even symmetry, and L_y odd, but the amplitude of the measured L_x is also an order of magnitude larger than L_y, as is predicted by the calculations (Fig. 1b). However, a closer inspection of L_y (top panel of Fig. 2b) reveals an unexpected oddity: the line of minimal amplitude of this signal is shifted by 0.3 μm from the center of the waveguide. This suggests that L_y not only contains a component with odd, but also a component with even symmetry. We therefore separate the signals according to their symmetries, by computing the signals with even symmetry, $L_{\mathrm{even}}(x,y)$, and odd symmetry, $L_{\mathrm{odd}}(x,y)$, as follows:

$$L_{\mathrm{even}}(x,y) = \frac{L(x,y) + L_{\mathrm{mir}}(x,y)}{2}, \tag{2a}$$

$$L_{\mathrm{odd}}(x,y) = \frac{L(x,y) - L_{\mathrm{mir}}(x,y)}{2}, \tag{2b}$$

where $L_{\mathrm{mir}}(x,y) = L(x_c - x, y)$ indicates the signal mirrored around the center x_c of the waveguide. We find x_c with an accuracy of 250 nm by fitting a peaked function to L_x. This uncertainty is caused by the low confinement of the model waveguide used. With increasing confinement this number will decrease. This approach is justified because $|E_x| >> |E_y|$. Hence, any appreciable shift of L_x due to mixing between the two channels would result in L_y being dominated by a component with even symmetry, which is clearly not the case.

In the middle and bottom panels of Fig. 2a and b we show the field maps with even and odd symmetry constructed with Eq. 2. We find that, as expected in L_x, the even symmetry component is much larger than the

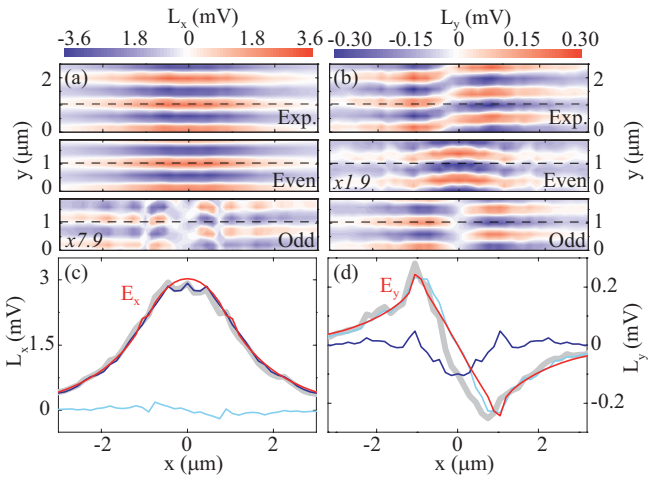

Fig. 2. (Color online) (a) and (b) Top panels: 2D maps of the real part of L_x and L_y, respectively. Middle and Bottom panels: 2D maps of the real part of the signals in L_x and L_y with even (Middle) and odd (Bottom) symmetry. In (a) and (b) the dashed black lines indicate the position of the line traces shown in (c) and (d), the multiplication factors refer to scaling of the colormap. (c) and (d) Line traces of the real part of the signal in L_x (c) and L_y (d) (indicated by the light grey lines), together with the even (dark blue lines) and odd (light blue lines) symmetry components, together with the fitted calculated in plane electric fields (red lines).

odd symmetry component. Furthermore, we observe that the minimum of the odd-symmetric signal in L_y is now on the center of the waveguide, and that L_y contains a non-negligible even-symmetric signal.

To gain more insight in our measurements, we inspect line traces (at a constant y) along the maxima of the signals with even and odd symmetry (Figs. 2c and d). As the 2D maps suggested, L_x is mainly even, with a negligible odd component. We attribute the signal with even symmetry in L_y to the presence of E_x and H_y in this channel. The presence of H_y or E_x in L_y, could be caused by mixing of the polarizations in the probe, the fiber or the detection path. We can place an upper bound on the amount of mixing by comparing the amplitude of the signal with even symmetry in L_x to that in L_y. From this comparison, we estimate that we detect $\sim 1/30$ of the signal from E_x and H_y in L_y (1/900 in intensity). Strikingly even such a small amount of mixing can distort L_y and, importantly, using Eq. 2 we can filter out this mixing.

Having shown how we can use symmetry considerations to identify the polarization mixing in our measurements, we now quantify the sensitivities of our system. In specific we use $\alpha'_{x,y}$ (Eq. 1) to fit the calculated in-plane electric fields to our measurements. From these fits we find that the relative sensitivity to the in-plane electric fields $\alpha'_x/\alpha'_y = 1.1 \pm 0.2 \pm 0.1$. Here, the first error indicates the range over which $\alpha'_{x,y}$ can vary before the sum of squares of the residual of the fit increases by a factor 2, and the second error follows from the 250 nm uncertainty in x_c. A comparison of the measurements to the magnetic field instead results in the same sensitivity ratio ($\beta'_y/\beta'_x = 1.2 \pm 0.2 \pm 0.3$). The difference in sensitivities could be explained by, for example, a slightly ovally shaped probe, a more sensitive detector in the x branch, or a slender tilt of the probe with respect to the sample.

Because the signal with even symmetry in L_y is smaller than the other signals and we understand its origin, we can use this channel to map an additional component of the near field. Hence, we now turn to the SRP measurements, where in addition to the in-plane electromagnetic components we also expect to detect signal from the out-of-plane component of the magnetic field. Here we orient the SRP such that the slit is parallel to x (as sketched in Fig. 1a) and light from H_z will contribute to L_y [4].

We confirm the detection of H_z by analyzing the amplitude of the standing wave pattern that results from a reflection of the end facet of the structure (inset of Fig. 3c). Because E_x and H_y do not experience a phase flip upon reflection, whereas H_z does, the standing wave of H_z is offset by a quarter wavelength compared to the standing wave of E_x and H_y. In our measurements (inset of Fig. 3c) we observe this shift, and accordingly detect H_z with L_y [4].

Having confirmed the detection of H_z, we now write the signals we expect to measure with the SRP as follows:

$$L_x \approx \alpha'_x E_x, \tag{3a}$$

$$L_y \approx \alpha'_y E_y + \gamma_y Z_0 H_z, \tag{3b}$$

where we use γ_y to quantify the sensitivity to the out-of-plane magnetic field.

We show the field maps measured with the SRP in the top panels of Fig. 3a and b. It is immediately evident that these 2D maps differ greatly from those measured with an AP (Fig. 2). Where with the AP L_y largely had an odd symmetry, we now mainly observe an L_y with even symmetry. Because we expect that the in-plane fields with odd symmetry still contribute to L_y, we again separate fields with even and odd symmetry in the signal from the two detectors. We show the resulting 2D maps in the middle and bottom panels of Fig. 3a and b. In contrast to the measurements with an AP (Fig. 2), these maps show that the dominant component of both L_x and L_y now has an even symmetry. At the same time, and in agreement with the measurements shown in Fig. 2, we only find a clear odd symmetry signal in L_y. That is, the symmetries of our measured near fields allow us to resolve three signals using only two detectors.

These findings are confirmed by the line traces of the separated signals that are shown in Fig. 3c and d. In these figure panels we see that the even symmetric component of L_x and both the even and odd sym-

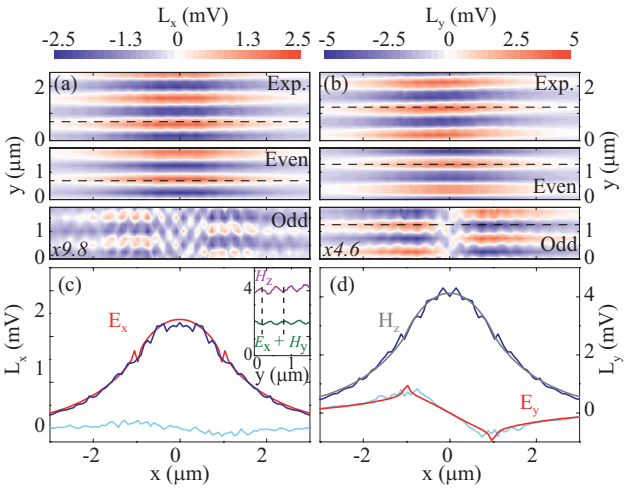

Fig. 3. (Color online) (a) and (b) Top panels: 2D maps of the the real part of L_x and L_y. Middle and bottom panels: 2D maps of the real part of the signals in L_x and L_y with even (Middle) and odd (Bottom) symmetry. The scaling of the bottom maps in (a) and (b) is indicated in the figures. (c) and (d) Line traces of the even (dark blue lines) and odd symmetry (light blue lines) components of L_x and L_y, together with the fitted calculated in-plane electric fields (red lines). In (c) the inset shows line traces of the amplitude of L_x (green) and L_y (purple) along $x = 0$. In (d) the dark grey line indicates H_z fitted to the signal in L_y with even symmetry.

metric components of L_y are in good agreement with the calculated distributions for E_x, H_z and E_y, respectively. By fitting these fields to the measurements, we find for the SRP that $\alpha_x/\alpha_y = 0.23 \pm 0.08 \pm 0.07$ and $\alpha'_x/\gamma_y = 0.94 \pm 0.50 \pm 0.05$. That is, the sensitivity to H_z is roughly equal to that of the superposition of E_x and H_y. Furthermore, the SRP is also relatively more sensitive to E_y than the AP. We explain the increased sensitivity by the slit that forms the gap in the SRP, because for y-polarized illumination there may exist an available mode in the slit, whereas for x-polarized illumination there is no available mode [15].

In this work we showed how symmetry can be used to identify and separate different electromagnetic field components in NSOM signals. By separating these fields, we opened up a new detection channel that allowed us to measure three near-field signals on only two detectors. That is, we mapped the out-of-plane magnetic field and two superpositions of the in-plane fields in two dimensions. In the future, we aim to extend this method, so that it can be used to measure all six components of the electromagnetic field. In combination with [13], this work allows for the simultaneous detection of five components of the optical near field. Because the only undetected field component is E_z, which in our study has odd symmetry, we aim to design a probe that in addition converts this last component to radiation on L_x. Such a probe, combined with the approach demonstrated in this work, would make the detection of complete nanoscale vector fields feasible. Lastly, the symmetries of the ridge waveguide are generally present in nanophotonic structures. Since measurement of the phase of the near-field signal is the only requirement enable the use symmetry for separating fields, we believe that our method will benefit different NSOM schemes, and experiments for a wide range of nanophotonic structures.

This work is part of the research programme of the Foundation for Fundamental Research on Matter (FOM), which is part of the Netherlands Organisation for Scientific Research (NWO). This work is supported by NanoNextNL of the Dutch ministry EL&I and 130 partners, and by the EU FET project SPANGL4Q.

References

1. C. F. Bohren and D. R. Huffman, *Absorption and scattering of light by small particles*, (John Wiley & Sons, 2008).
2. K. Sakoda, *Optical properties of photonic crystals*, (Springer-Verlag, 2005).
3. R. L. Olmon, M. Rang, P. M. Krenz, B. A. Lail, L. V. Saraf, G. D. Boreman, and M. B. Raschke, Phys. Rev. Lett. **105**, 167403 (2010).
4. M. Burresi, D. van Oosten, T. Kampfrath, H. Schoenmaker, R. Heideman, A. Leinse, and L. Kuipers, Science **326**, 550 (2009).
5. T. Bauer, S. Orlov, U. Peschel, P. Banzer, and G. Leuchs, Nature Photonics **8**, 23 (2014).
6. H. W. Kihm, S. M. Koo, Q. H. Kim, K. Bao, J. E. Kihm, W. S. Bak, S. H. Eah, C. Lienau, H. Kim, P. Nordlander, N.J. Halas, N.K. Park, and D.S. Kim, Nature Communications **2**, 451 (2011).
7. M. Burresi, R. J. P. Engelen, A. Opheij, D. van Oosten, D. Mori, T. Baba, and L. Kuipers, Phys. Rev. Lett. **102**, 033902 (2009).
8. P. Uebel, M. A. Schmidt, H. W. Lee, and P. S. J. Russell, Optics express **20**, 28409 (2012).
9. M. Schnell, A. García-Etxarri, J. Alkorta, J. Aizpurua, and R. Hillenbrand, Nano letters **10**, 3524 (2010).
10. M. Schnell, A. García-Etxarri, A. J. Huber, K. Crozier, J. Aizpurua, and R. Hillenbrand, Nature Photonics **3**, 287 (2009).
11. J. Dorfmüller, D. Dregely, M. Esslinger, W. Khunsin, R. Vogelgesang, K. Kern, and H. Giessen, Nano letters **11**, 2819 (2011).
12. P. Venugopalan, Q. Zhang, X. Li, and M. Gu, Optics Express **21**, 15247 (2013).
13. B. le Feber, N. Rotenberg, D. M. Beggs, and L. Kuipers, Nature Photonics **8**, 43 (2014).
14. J. D. Joannopoulos, S. G. Johnson, J. N. Winn, and R. D. Meade, *Photonic crystals: molding the flow of light*, (Princeton university press, 2008).
15. F. J. Garcia-Vidal, L. Martin-Moreno, T. Ebbesen, and L. Kuipers, Reviews of Modern Physics **82**, 729 (2010).

Informational Fifth Page

References

1. C. F. Bohren and D. R. Huffman, *Absorption and scattering of light by small particles*, (John Wiley & Sons, 2008).
2. K. Sakoda, *Optical properties of photonic crystals*, vol. 80 (Springer-Verlag, 2005).
3. R. L. Olmon, M. Rang, P. M. Krenz, B. A. Lail, L. V. Saraf, G. D. Boreman, and M. B. Raschke, "Determination of electric-field, magnetic-field, and electric-current distributions of infrared optical antennas: A near-field optical vector network analyzer," Phys. Rev. Lett. **105**, 167403 (2010).
4. M. Burresi, D. van Oosten, T. Kampfrath, H. Schoenmaker, R. Heideman, A. Leinse, and L. Kuipers, "Probing the magnetic field of light at optical frequencies," Science **326**, 550–553 (2009).
5. T. Bauer, S. Orlov, U. Peschel, P. Banzer, and G. Leuchs, "Nanointerferometric amplitude and phase reconstruction of tightly focused vector beams," Nature Photonics **8**, 23–27 (2014).
6. H. W. Kihm, S. M. Koo, Q. H. Kim, K. Bao, J. E. Kihm, W. S. Bak, S. H. Eah, C. Lienau, H. Kim, P. Nordlander, N.J. Halas, N.K. Park, and D.S. Kim, "Bethe-hole polarization analyser for the magnetic vector of light," Nature Communications **2**, 451 (2011).
7. M. Burresi, R. J. P. Engelen, A. Opheij, D. van Oosten, D. Mori, T. Baba, and L. Kuipers, "Observation of polarization singularities at the nanoscale," Phys. Rev. Lett. **102**, 033902 (2009).
8. P. Uebel, M. A. Schmidt, H. W. Lee, and P. S. J. Russell, "Polarisation-resolved near-field mapping of a coupled gold nanowire array," Optics express **20**, 28409–28417 (2012).
9. M. Schnell, A. García-Etxarri, J. Alkorta, J. Aizpurua, and R. Hillenbrand, "Phase-resolved mapping of the near-field vector and polarization state in nanoscale antenna gaps," Nano letters **10**, 35243528 (2010).
10. M. Schnell, A. García-Etxarri, A. J. Huber, K. Crozier, J. Aizpurua, and R. Hillenbrand, "Controlling the near-field oscillations of loaded plasmonic nanoantennas," Nature Photonics **3**, 287–291 (2009).
11. J. Dorfmüller, D. Dregely, M. Esslinger, W. Khunsin, R. Vogelgesang, K. Kern, and H. Giessen, "Near-field dynamics of optical yagi-uda nanoantennas," Nano letters **11**, 2819–2824 (2011).
12. P. Venugopalan, Q. Zhang, X. Li, and M. Gu, "Polarization-sensitive characterization of the propagating plasmonic modes in silver nanowire waveguide on a glass substrate with a scanning near-field optical microscope," Optics Express **21**, 15247–15252 (2013).
13. B. le Feber, N. Rotenberg, D. M. Beggs, and L. Kuipers, "Simultaneous measurement of nanoscale electric and magnetic optical fields," Nature Photonics **8**, 43–46 (2014).
14. J. D. Joannopoulos, S. G. Johnson, J. N. Winn, and R. D. Meade, *Photonic crystals: molding the flow of light* (Princeton university press, 2008).
15. F. J. Garcia-Vidal, L. Martin-Moreno, T. Ebbesen, and L. Kuipers, "Light passing through subwavelength apertures," Reviews of Modern Physics **82**, 729 (2010).